Electrochemically Derived Redox Molecular Architecture: A Novel Electrochemical Interface for Voltammetric Sensing

Ramendra Sundar Dey, Susmita Gupta, Rupankar Paira, and C. Retna Raj*

Department of Chemistry, Indian Institute of Technology, Kharagpur 721 302, India

ABSTRACT Redox-active molecular architectures are electrochemically derived on the electrode surface by Michael addition reaction of *o*-quinone with surface adsorbed nucleophiles. Electrogenerated *o*-quinone undergoes facile Michael addition reaction with nucleophile mercaptotriazole (MTz) and mercaptoimidazole (MIm) preassembled on Au electrode. The Michael addition reaction yields redox molecular architectures of 4-(3-mercapto-[1,2,4]triazol-1-yl)-benzene-1,2-diol (MTBD) and 4-(2-mercapto-imidazol-1-yl)-benzene-1,2-diol (MIBD). Solution pH controls the Michael addition reaction; the reaction of *o*-quinone with MTz nucleophile is more favorable in neutral pH whereas it is favorable in pH ≥9 with MIm. Michael addition of electrogenerated *o*-quinone with the nucleophile is quantitatively followed in real time using electrochemical quartz crystal microbalance (EQCM). The redox molecular architecture on the electrode surface is characterized by attenuated total reflection (ATR) spectral and electrochemical measurements. ATR spectral measurement confirms the Michael addition with the nucleophile. The redox molecular architecture displays reversible voltammetric response at 0.2 V corresponding to the redox reaction surface confined catechol moiety. The surface coverage of MTBD and MIBD on the electrode surface at pH 7.2 is estimated to be $(5.4 \pm 0.2) \times 10^{-10}$ and $(2.0 \pm 0.2) \times 10^{-10}$ mol/cm^2, respectively. Both redox molecular assemblies efficiently mediate the oxidation of reduced nicotinamide adenine dinucleotide (NADH) at a favorable potential. A large decrease in the overpotential associated with an enhancement in the voltammetric peak current with respect to the unmodified electrode is observed. Flow injection amperometric sensing of NADH is performed at the potential of 230 mV. These modified electrodes could detect NADH at micromolar level. Mixed molecular architecture of cysteamine (CYST) and MTz/MIm are developed for the interference free voltammetric sensing of NADH.

KEYWORDS: redox molecular architecture • nucleophile • Michael addition • EQCM • flow injection • NADH • sensing

INTRODUCTION

Tailoring of electrochemical interface with redox molecular assemblies is one of the fascinating approaches in developing versatile platforms for catalytic and sensing applications. The surface adsorbed redox molecules have important role in controlling the electron transfer reaction at the interface. Various attempts have been made to design such interface using redox active organic polymers, transition metal complexes etc. (1). The chemically synthesized redox active organothiols have been traditionally used to develop molecular architectures on the coinage metal surface. Compact and well ordered redox monolayer assembly can be prepared on Au surface by the chemisorption of thiol terminal groups (2). The strong intermolecular interaction assures the stability and compactness of these molecular architectures. Unlike the polymer-modified electrodes, fast electron transfer and high selectivity and sensitivity can be achieved under optimized conditions with the molecular architectures based electrochemical platform. Such molecular architectures find potential application in the area of electroanalytical chemistry (3). For instance, Willner and co-workers have extensively used self-assembling approach for the development of biosensing interfaces (4). Redox active monolayer assemblies such as quinone, viologen, microperoxidase-11, etc., have been investigated (2, 5). Molecular self-assembly assisted electrical wiring of redox enzyme for the development of biosensors has been demonstrated (6). Electrochemical sensors and biosensors for the sensing of bioanalytes, heavy metals etc. have also been developed using chemically synthesized redox active molecular self-assemblies of organothiols (4, 7−10).

Nicotinamide adenine dinucleotide (NAD^+) is an enzyme cofactor required for the function of more than 300 dehydrogenase based enzyme in living system (11). The function of NAD^+ dependent dehydrogenase biosensing device is based on the quantification of enzymatically generated NADH during the reaction. The concentration of enzymatically generated NADH is directly proportional to the amount of substrate present in the sample. Although the redox potential of NAD^+/NADH couple is −0.56 V vs SCE at pH 7 (12), oxidation of NADH on conventional electrodes require high positive potential as large as 0.8−1 V, because of the slow electron transfer and associated dimerization of intermediates produced (13). Several methodologies have been adopted to facilitate the electron transfer reaction and to decrease the overpotential (11).

The redox mediator based electrodes have been traditionally used to facilitate the oxidation of NADH (11, 14, 15).

* Corresponding author. E-mail: crraj@chem.iitkgp.ernet.in. Fax: 91-3222-282522.

Received for review January 10, 2010 and accepted April 15, 2010

DOI: 10.1021/am1000213

Willner and co-workers have developed electrochemical NADH transducer based on the self-assembly of pyrroloquinoline quinone (16). Abruna and co-workers exploited electrochemically derived redox polymers for the electrocatalytic oxidation of NADH and development of dehydrogenase based biosensors (14, 15). Wang and co-workers for the first time demonstrated the facilitated oxidation of NADH on carbon nanotube (CNT) based electrodes without any redox mediator (17). Gorski and co-workers have reported the mediated oxidation of NADH and development of biosensors using CNT-redox mediator and treated CNT based electrodes (18−20). Xie and co-workers followed Gorski's approach and prepared NADH transducer using chitosan-dopamine-CNT nanocomposite (21). The CNTs functionalized with redox relay has been successfully used for the sensing of NAD(P)H/NADH and for the fabrication of biosensors (22, 23). Recently, Milczare has reported the electrocatalytic oxidation of NADH using lignosulfonate modified electrodes (24). It is generally accepted that quinones and diimines are the potential mediators in the oxidation of NADH (11). Our group is interested in the development of electrochemical interfaces for the development of dehydrogenase based biosensors and we have demonstrated the catalytic effect of redox functionalized molecular self-assemblies and nanomaterials in the oxidation of NADH (25−27). Recently, we have reported the electrochemical generation of redox mediator on the self-assemblies of thiouracil and mercaptopurines on Au electrode and the electrocatalytic oxidation of NADH and ascorbate (AA) (26, 28). Although the redox mediator could mediate the oxidation of NADH at less positive potential, the sensitivity of the electrode is low, as the surface coverage (Γ) of the redox mediator on the electrode surface is relatively less (1×10^{-11} mol/cm^2). Moreover, presence of AA strongly interfere the measurement of NADH, as the oxidation of both AA and NADH occurs almost at the same potential (28). The concentration of NADH cannot be quantified with this electrode in the presence of interfering AA, as the mediator mediates the oxidation of both NADH and AA. In continuation of our efforts to develop a suitable electrochemical interface for the interference free sensing of NADH, herein we describe the generation of redox molecular architecture by the reaction of *o*-quinone with the surface adsorbed nucleophiles such as MTz and MIm and the electrocatalytic sensing of NADH by flow injection amperometric method. Interestingly, we could obtain a high Γ value of the redox molecular assembly and achieve interference free voltammetric sensing of NADH. The generation of redox molecular architecture is quantitatively followed by EQCM and spectral measurements.

METERIALS AND METHODS

Chemicals. NADH, MTz, MIm, catechol (CA), AA, and CYST were obtained from Sigma-Aldrich and were used as received. All other chemicals used in this investigation were of analytical grade. Phosphate buffer solution (0.1 M) of pH 7.2 was used as supporting electrolyte in all electrocatalytic experiments. For voltammetric measurements at different pH, 0.1 M Na_2HPO_4 or NaH_2PO_4 with H_3PO_4 were used as supporting electrolytes. All the solutions were prepared using Millipore water (Milli-Q system).

Instrumentation. Voltammetric measurements were performed with CHI643B electrochemical analyzer attached with a Faraday cage/picoampere booster (CHI, Austin, TX). A two-compartment three-electrode cell with a polycrystalline Au working electrode (BAS, 2 mm diameter), a platinum wire auxiliary electrode and an Ag/AgCl (3 M KCl) reference electrode was used for all the voltammetric measurements. All the potentials in this study are referred against this reference electrode unless otherwise mentioned. The mass change at the electrode surface during the Michael addition reaction of *o*-quinone with surface adsorbed nucleophile was quantified using CHI400A computer controlled time-resolved EQCM (CHI, Austin, TX). AT-cut quartz crystals covered with Au deposited on a Cr layer, having fundamental resonant frequency of 8 MHz, was used as the working electrode. The area of Au covered quartz crystal was 0.196 cm^2. A single-compartment Teflon cell with a platinum wire auxiliary electrode and Ag/AgCl (3 M KCl) reference electrode was used. The Au coated quartz crystal was electrochemically pretreated by sweeping the potential from −0.2 to 1.5 V in 0.025 M H_2SO_4. The electrode was then washed with Millipore water and used in EQCM studies. The flow injection analysis experiments were carried out with a CHI842B dual channel electrochemical analyzer (CHI, Austin, TX) and a flow cell (BAS) of 5 μL volume. The flow rate of the mobile phase (phosphate buffer of pH 7.2) was controlled by BAS LC peristaltic pump (PM-80) with Teflon tubing. A Rheodyne 7125 injector with a 20 μL stainless steel injection loop was used for sample injection. The electrode potential was held at 230 mV and 40 μL of NADH was injected at regular intervals. ATR spectral measurements of the molecular assemblies were recorded using Omnic FT-IR spectrometer (NEXUS-870). Au coated microscopic glass slides were used as substrate for ATR spectral measurements.

Procedure. Polycrystalline Au electrodes were polished repeatedly with fine emery paper and alumina powder (0.06 μM) and sonicated in water for 5−10 min. The polished electrodes were then electrochemically cleaned by cycling the potential between −0.2 and 1.5 V in 0.25 M H_2SO_4 at the scan rate of 10 V/s for 10 min or until the characteristic cyclic voltammogram for an Au electrode was obtained. The pretreated Au electrode was then immersed in ethanolic solution of MTz or MIm (1 mM) for a period of 2 h at room temperature for the self-assembling of respective thiols. Hereafter, the Au electrode modified with the nucleophiles of MTz and MIm will be referred as Au-MTz and Au-MIm, respectively. The monolayer modified Au electrodes were then washed extensively with ethanol and water to remove the physically adsorbed nucleophiles and subjected to electrochemical measurements. The mixed molecular architecture was obtained by soaking the redox molecular architecture based electrode in 1 mM CYST for a period of 2 h. The real surface area of the polycrystalline Au electrode (0.0389 cm^2) was determined from the charge consumed during the reduction of surface oxides; the value of 400 μC/cm^2 reported in the literature was used in the calculations (29). The real surface area of the electrodes was used in the calculation of surface coverage of the redox molecular architecture. For ATR spectral measurements, the Au-coated glass slide was soaked in absolute ethanol for 15 min and then washed with Millipore water repeatedly. The clean substrates were then immersed in ethanol solution of MTz (1 mM) for a period of 2 h at room temperature and the Michael addition was performed in phosphate buffer solution as described earlier.

RESULTS AND DISCUSSION

Electrochemical Generation of Redox Molecular Architecture. The redox molecular architecture on the electrode surface was electrochemically generated by the

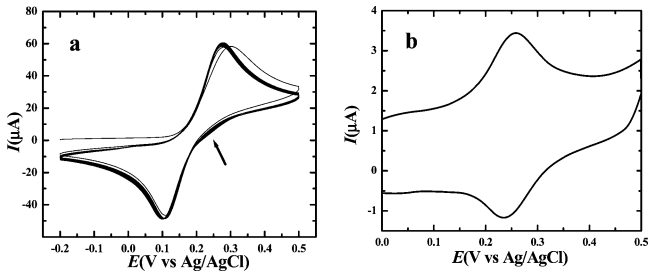

FIGURE 1. Cyclic voltammogram obtained for (a) Au-MTz electrode during the potential cycling between −0.2 to 0.5 V in phosphate buffer solution (pH 7.2) containing 0.5 mM CA; scan rate 100 mV/s. (b) Voltammetric response of the same electrode after potential cycling in fresh phosphate buffer solution without CA; scan rate 50 mV/s. Arrow in panel a indicates the appearance of new hump during the potential cycling.

reaction of *o*-quinone with surface adsorbed nucleophiles, MTz and MIm. The redox reaction of CA involves 2e and $2H^+$ and *o*-quinone is generated during its oxidation. A quasi reversible voltammetric response with an $E_{1/2}$ value of 0.18−0.2 V and peak-to-peak separation (ΔE_p) of 150−200 mV was obtained for the redox reaction of CA at the MTz and MIm molecular self-assemblies. A small hump at ~0.25 V appeared while cycling the potential of the electrode between −0.2 and 0.5 (Figure 1a). The magnitude of the main peak decreases while increasing the cycling time. These electrodes (Au-MTz and Au-MIm) after potential cycling displayed well-defined reversible voltammetric response at ~0.23 V, characteristic of a surface-confined redox species when they were transferred to phosphate buffer solution without CA (Figure 1b). The quinones are known to undergo Michael addition reaction with dissolved nucleophiles in homogeneous solution (30−32). The close examination of the chemical structure of the molecular assemblies on the electrode surface shows that both MTz and MIm have one ionizable proton at N(1) position (see the Supporting Information). The electrochemically generated *o*-quinone can undergo facile Michael addition reaction, if the N(1) position of the nucleophile is deprotonated. The MTz and MIm self-assemblies are believed to be fully or partially ionized in neutral aqueous solution. The voltammetric features obtained during the potential cycling (Figure 1a) suggests that the electrogenerated *o*-quinone undergo Michael addition reaction with the surface adsorbed nucleophile at the N(1) position according to the mechanism (Scheme 1). The Michael addition reaction yield redox molecular architectures of 4-(3-mercapto-[1,2,4]triazol-1-yl)-benzene-1,2-diol (MTBD) and 4-(2-mercapto-imidazol-1-yl)-benzene-1,2-diol (MIBD) on the Au-MTz and Au-MIm electrodes, respectively (Scheme 1). The MTBD and MIBD redox molecular architectures can undergo 2e, $2H^+$ redox reaction and show reversible voltammetric response due to the presence of the *o*-quinone functionality.

The Michael addition reaction of electrogenerated *o*-quinone with the surface adsorbed nucleophile is strongly dependent on the solution pH. For the facile Michael addition reaction, the N(1) position should be deprotonated. To examine the influence of pH, the reaction was performed at different pH and surface coverage of the redox molecular

Scheme 1. Scheme Depicting the pH-Dependent Michael Addition Reaction of Electrogenerated *o*-Quinone and Generation of Redox Molecular Architecture

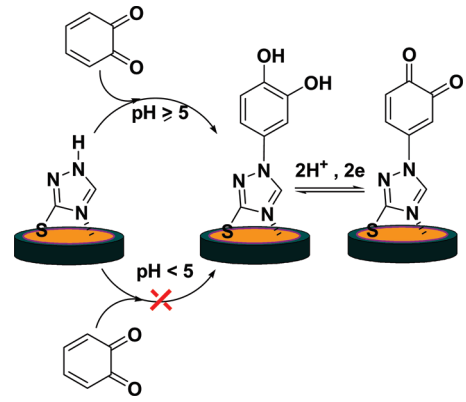

architecture was estimated from the voltammograms. The surface coverage of molecular architecture gradually increases with the solution pH. In the case of MTz, high surface coverage was obtained when the Michael addition was carried out at pH 7.2. On the other hand, MIm monolayer yields maximum surface coverage at pH 9 (see the Supporting Information). This is due to the difference in the surface pK_a of the self-assemblies. The solution pH controls the Michael addition reaction of electrogenerated quinone with surface adsorbed nucleophile. The Michael addition reaction is not favorable in acidic pH due to the protonation of N(1) position of MTz and MIm. The surface pK_a of MTz and MIm can be conveniently calculated from the plot of pH vs surface coverage. The surface pK_a of MTz and MIm self-assemblies was calculated to be 4.9 and 6.7, respectively.

Electrochemical Quartz Crystal Microbalance Studies. EQCM techniques can be used to quantify the change in mass on the electrode surface in real time by measuring the changes in frequency of the quartz crystal. The frequency change can be related to the mass according to the Sauerbrey equation (33)

$$\Delta f = -\frac{2f_0^2 \Delta m}{[A\sqrt{(\mu\rho)}]}$$

where f_0 is the resonant frequency of fundamental mode of the crystal (8 MHz), A is the area of Au-deposited quartz crystal (0.196 cm^2), μ is the shear modulus of quartz (2.95×10^{11} g/cm s^2), and ρ is the density of crystal (2.684 g/cm^3). The electrochemically driven Michael addition reaction of *o*-quinone with the surface adsorbed nucleophile was followed by monitoring the frequency change during the reaction. Figure 2 represents the typical EQCM response obtained during Michael addition reaction of *o*-quinone with self-assembly of MTz. The potential of the crystal modified with MTz was cycled between −0.2 to 0.5 V at the sweep rate of 100 mV/s in the presence of CA (0.5 mM). Gradual decrease in frequency was noticed during the course of the reaction. The decrease in the frequency is ascribed to the

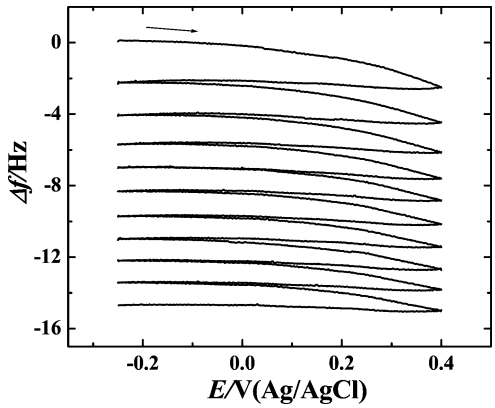

FIGURE 2. Frequency−potential response obtained for Au-MTz electrode during the potential cycling in phosphate buffer solution (pH 7.2) containing 0.5 mM CA; scan rate 100 mV/s.

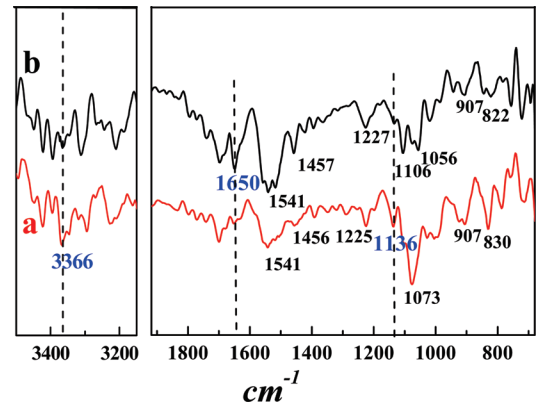

FIGURE 3. ATR spectra of (a) MTz and (b) MTBD molecular architectures. Selected regions are given for clarity reason.

increase in mass at the electrode surface due to the Michael addition reaction. Similar response was also obtained with MIm self-assembly (see the Supporting Information). The overall mass change was calculated using Sauerbrey equation and was 104.2 ± 0.8 and 83.4 ± 0.6 ng/cm^2 on the MTz and MIm self-assemblies, respectively. No such change in the frequency was observed with the unmodified crystal, confirming that the change observed with the self-assemblies is due to the Michael addition reaction of electrogenerated *o*-quinone. The number of CA molecules reacted with the MTz and MIm self-assemblies were calculated to be 5.7 × 10^{14} and 4.5 × 10^{14}, respectively. The number of MTz and MIm self-assemblies on the electrode surface were obtained from the reductive desorption in alkaline solution and it was 10.5 × 10^{14} and 5.5 × 10^{14}, respectively. It is apparent that all MTz nucleophiles on the electrode surface could not undergo Michael addition reaction. However, almost all MIm nucleophiles underwent the reaction. The surface orientation and conformation of these nucleophiles on the electrodes surface could be the reason for the observed difference.

Electrochemical Characterization of Redox Molecular Architectures. The electrochemically derived molecular architectures, MTBD and MIBD display well-defined voltammetric response for the redox reaction of catechol/quinone redox couple. The ΔE_p is typically small although not zero, implying fast electron transfer kinetics. The surface coverage of MTBD and MIBD was obtained by integrating the area under anodic peak and was (5.4 ± 0.2) × 10^{-10} and (2.0 ± 0.2) × 10^{-10} mol/cm^2, respectively. It should be pointed out here that the surface coverage obtained for the redox mediator is significantly higher than those of our earlier reports (19, 21). Unlike the other heterocyclic thiols (mercaptopurine and thiouracil), the steric hindrance for the approach of electrogenerated quinone cannot be expected in the present cases. The electrogenerated *o*-quinone can easily approach the nucleophile on the electrode surface for the reaction. The anodic peak potential (E_p^a) of surface confined MTBD and MIBD shifts negatively while increasing the solution pH. The plot of E_p^a vs pH is linear with a slope of 65 ± 2 mV suggesting the involvement of electron and proton at 1:1 ratio (see the Supporting Information). The slope is slightly higher than for an ideal surface confined catechol/quinone redox couple. The standard rate constant (k_s) for the redox reaction of Michael addition product on the electrode surface was obtained using Laviron approach. The ΔE_p value was <200 mV at high scan rate and the k_s value of MTBD and MIBD was calculated to be 63.5 ± 0.5 and 56.5 ± 0.5 s^{-1}, respectively.

ATR Spectral Studies. The redox molecular architecture on the electrode surface was further characterized by ATR spectral measurements. Figure 3 is the ATR spectral profile obtained for the MTz and MTBD assemblies on the electrode surface. The spectral bands were assigned according to the earlier reports (34−39). The band observed at 907 cm^{-1} is assigned for C−S stretching (34, 35). The absence of S−H stretching vibration indicates that the molecular assemblies chemisorbed onto the electrode surface. The intensity of the band at 1136 cm^{-1} corresponding to N−H deformation (37) and the band at 3366 cm^{-1} corresponding to N−H stretching (37) on the MTz molecular assembly significantly decreased after the Michael addition reaction, supporting the involvement of this nitrogen in the Michael addition reaction. The band observed at 1541 cm^{-1} is ascribed to the stretching vibration of C═N (34−36). The molecular assembly MTBD is expected to show characteristic band for —OH group of catechol moiety. Such characteristic band was not observed for MTBD. However, we observed a new band at 1650 cm^{-1}, which is characteristic of C═O (38). The catechol is known to undergo autoxidation to the corresponding quinone in air (39). We suggest that the band observed at 1650 cm^{-1} can be due to the C═O generated on the electrode surface by the autoxidation of the catechol moiety of MTBD. The complete assignment of the peaks is given in the Supporting Information (Table S1).

Electrocatalytic Sensing of NADH. Figure 4A displays the electrocatalytic response of MTBD electrode toward oxidation of NADH. The dramatic enhancement of anodic peak associated with a decrease in the cathodic peak of surface confined mediator in the presence of NADH indicates the strong electrocatalytic effect of the mediator. The oxidized form of the mediator efficiently reacts with the NADH to produce NAD$^+$ and then convert to the reduced form of the mediator (Figure 4B). Significant (~600 mV) decrease in the overpotential with respect to the unmodified electrode is observed with the molecular architecture-based

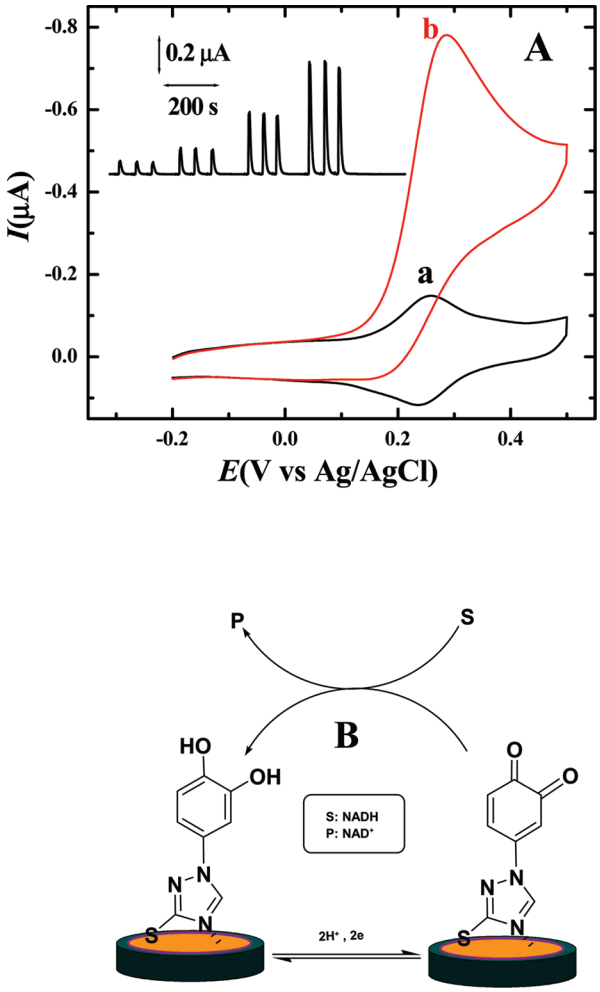

FIGURE 4. (A) Cyclic voltammograms illustrating the electrocatalytic activity of redox molecular architecture in the mediated oxidation of NADH in phosphate buffer solution (pH 7.2): (a) in the absence and (b) in the presence of NADH (0.5 mM). Scan rate: 10 mV/s. Inset shows the flow injection amperometric response upon repetitive injection of 20 μL of (a) 10, (b) 20, (c) 40, and (d) 80 μM NADH. Electrode potential: 0.23 V. Mobile phase: 0.1 M phosphate buffer solution (pH 7.2). Flow rate: 1 mL/min. (B) Scheme illustrating the mediated electrocatalytic oxidation of NADH by the redox molecular architecture.

electrode. The catalytic peak current linearly increases with square root of sweep rate, pointing out that the electrocatalytic reaction is diffusion-controlled (see the Supporting Information). The voltammetric response of the electrode is very stable in the subsequent sweeps, though a slight decrease was observed in the first few sweeps. A gradual increase in the voltammetric peak current was obtained upon the addition of NADH. The electrode shows linear response up to 80 μM and has a dynamic range up to 0.15 mM (see the Supporting Information). The performance of the electrode was further examined with amperometric flow injection analysis. The electrode potential was held at 230 mV and 20 μL of NADH of different concentrations was injected at regular intervals. Stable amperometric response was obtained upon repeated injection of NADH (Figure 4A inset). The sensitivity and limit of detection of the electrode was calculated to be 172.75 $\pm$ 0.05 μA mM^{-1} cm^{-2} and 0.5 μM, respectively. The response time of the electrode was 1 s.

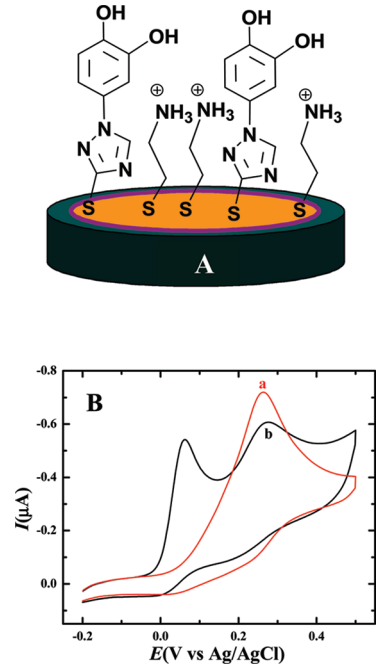

FIGURE 5. (A) Mixed molecular architecture of MTBD and CYST on Au electrode (B) Cyclic voltammograms obtained for the oxidation of NADH (0.05 mM) in presence of AA (0.05 mM) on (a) the MTBD and (b) the mixed molecular architecture of MTBD and CYST.

The current response upon repetitive injection of NADH was constant, confirming that the electrode has a good operational stability. This electrode is stable for 1 day when it is stored in phosphate buffer solution of pH 7.2. The MIBD molecular architecture has showed similar electrocatalytic response (see the Supporting Information).

The interference due to AA is one of the major challenges in the voltammetric sensing of NADH. The redox molecular architecture based electrodes show only one voltammetric peak for AA and NADH in their coexistence (Figure 5B), indicating that the concentration of NADH cannot be monitored in the presence of AA. Enzyme ascorbate oxidase and negatively charged polymer like nafion were conventionally used to mitigate the interference due to AA (14, 40). However, the negatively charged nafion would hinder the approach of anionic NADH and immobilization of enzyme ascorbate oxidase involves the use of additional reagents. Another interesting approach to mitigate the interference is the use of mixed molecular self-assembly (41). We have developed the mixed molecular architecture of CYST and MTBD/MIBD (Figure 5A) for the sensing of NADH in the presence of AA without interference. The mixed molecular architecture shows separate voltammetric signal for NADH and AA at the potential of 275 and 60 mV, respectively (Figure 5B). It indicates that the concentration of NADH can be measured using the mixed self-assembly without interference from AA. As the separation between the voltammetric peaks is ~215 mV, it is possible to determine the concentration of NADH without interference from AA by voltammetry. The peak potential for the oxidation of NADH on the MTBD-CYST mixed molecular architecture modified electrode remained same as in the case of MTBD electrode. The self-assembly of CYST is known to favor the oxidation of

ascorbate at less positive potential (42) due to the electrostatic interaction. Oxidation of AA occurs well before the oxidation of NADH on the mixed self-assembly, presumably because of favorable interaction of negatively charged AA with positively charged CYST.

CONCLUSION

The Michael addition reaction of electrochemically derived *o*-quinone with surface adsorbed nucleophile yields redox active molecular architecture. The solution pH controls the Michael addition reaction on the electrode surface. EQCM and ATR measurements confirm the Michael addition of quinone with the molecular assembly on the electrode surface. The catechol/quinone moiety of the molecular architecture shows reversible voltammetric response. The redox molecular architectures efficiently mediate the oxidation of NADH at less positive potential. Flow injection amperometric sensing of NADH using the redox molecular architecture has been performed. Mixed molecular architecture has been developed for the interference free sensing of NADH. The mixed molecular architecture show individual voltammetric peaks for NADH and AA. The redox molecular architectures generated by the Michael addition reaction are very promising for the development of electrochemical dehydrogenase biosensors.

Acknowledgment. This work was supported by Department of Science and Technology (DST), New Delhi. R.S.D. thanks UGC for a research fellowship.

Supporting Information Available: Figures S1−S10, including the structure of MTz and MIm, cyclic voltammogram of MIBD and its catalytic activity toward NADH, frequency potential response of MIm during MA, cyclic voltammetric response of MIBD toward NADH in presence of AA; Table S1 summarizing the ATR spectral assignment for MTz and MTBD (PDF). This material is available free of charge via the Internet at http://pubs.acs.org.

REFERENCES AND NOTES

(1) Bard, A. J.; Faulkner, L. R. *Electrochemical Methods—Fundamentals and Applications*; John Wiley and Sons: New York, 2000; p 580.
(2) Finklea, H. O. In *Electroanalytical Chemistry*; Bard, A. J., Rubinstein, I., Eds.; Marcel Dekker: New York, 1996; Vol. 19, pp 109−335.
(3) Murray, R. W.; Bard, A. J. In *Electroanalytical Chemistry*; Marcel Dekker: New York, 1984; Vol. 13, p 191.
(4) Willner, I.; Katz, E. *Angew. Chem., Int. Ed.* **2000**, *39*, 1180–1218.
(5) Katz, E.; Willner, I. *Langmuir*. **1997**, *13*, 3364–3373.
(6) Xiao, Y.; Patolsky, F.; Katz, E.; Hainfeld, J. F.; Willner, I. *Science* **2003**, *299*, 1877–1881.
(7) Casero, E.; Darder, M.; Takada, K.; Abruna, H. D.; Pariente, F.; Lorenzo, E. *Langmuir* **1999**, *15*, 127–134.
(8) Gobi, K. V.; Kitamura, F.; Tokuda, K.; Ohsaka, T. *J. Phys. Chem. B.* **1999**, *103*, 83–88.
(9) Raj, C. R.; Kitamura, F.; Ohsaka, T. *Langmuir* **2001**, *17*, 7378–7386.
(10) Tian, Y.; Mao, L.; Okajima, T.; Ohsaka, T. *Anal. Chem.* **2002**, *74*, 2428–2434.
(11) Gorton, L.; Dominguez, E. Electrochemistry of NAD(P)+/NAD(P)H. In *Encyclopedia of Electrochemistry, Bioelectrochemistry*; Wilson, G. S., Ed.; Wiley−VCH: Weinheim, Germany, 2002; Vol. 9, pp 67−143, and the references cited therein.
(12) Clark, W. M. *Oxidation−reduction Potentials of Organic Synthesis*; RE Krieger Publishing: Huntington, NY, 1972.
(13) Blaedel, W. J.; Jenkins, R. A. *Anal. Chem.* **1975**, *47*, 1337–1343.
(14) Pariente, F.; Tobalina, F.; Moreno, G.; Herna' ndez, L.; Lorenzo, E.; Abrun˜a, H. D. *Anal. Chem.* **1997**, *69*, 4065–4075.
(15) Wu, Q.; Maskus, M.; Pariente, F.; Tobalina, F.; Ferna' ndez, V. M.; Lorenzo, E.; Abrun˜a, H. D. *Anal. Chem.* **1996**, *68*, 3688–3696.
(16) Willner, I.; Riklin, A. *Anal. Chem.* **1994**, *66*, 1535–1539.
(17) Musameh, M.; Wang, J.; Merkoci, A.; Lin, Y. *Electrochem. Commun.* **2002**, *4*, 743–746.
(18) Zhang, M.; Gorski, W. *J. Am. Chem. Soc.* **2005**, *127*, 2058–2059.
(19) Wooten, M.; Gorski, W. *Anal. Chem.* **2010**, *82*, 1299–1304.
(20) Zhang, M.; Gorski, W. *Anal. Chem.* **2005**, *77*, 3960–3965.
(21) Ge, B.; Tan, Y.; Xie, Q.; Ma, M.; Yao, S. *Sens. Actuators, B* **2009**, *137*, 547–554.
(22) Yan, Y. M.; Yehezkeli, O.; Willner, I. *Chem.—Eur. J.* **2007**, *13*, 10168–10175.
(23) Chakraborty, S.; Raj, C. R. *J. Electroanal. Chem.* **2007**, *609*, 155–162.
(24) Milczarek, G. *Langmuir* **2009**, *25*, 10345–10353.
(25) Jena, B. K.; Raj, C. R. *Chem. Commun.* **2005**, *15*, 2005–2007.
(26) Behera, S.; Raj, C. R. *Langmuir* **2007**, *23*, 1600–1607.
(27) Chakraborty, S.; Raj, C. R. *Electrochem. Commun.* **2007**, *9*, 1323–1330.
(28) Behera, S.; Sampath, S.; Raj, C. R. *J. Phys. Chem. C.* **2008**, *112*, 3734–3740.
(29) Trasatti, S.; Petrii, O. A. *Pure Appl. Chem.* **1991**, *63*, 711–734.
(30) Nematollahi, D.; Goodarzi, H. *J. Org. Chem.* **2002**, *67*, 5036–5039.
(31) Nematollahi, D.; Tammari, E. *J. Org. Chem.* **2005**, *70*, 7769–7772.
(32) Shahrokhian, S.; Amiri, M. *Electrochem. Commun.* **2005**, *7*, 68–73.
(33) Sauerbrey, G. Z. *Phys.* **1959**, *155*, 206–222.
(34) Krishnakumar, V.; Xavier, R. J. *Spectrochim. Acta, A* **2004**, *60*, 709–714.
(35) Venter, M. M.; Zaharia, V. *Studia Univ. Babes-Bolyai, Chem/* **2007**, *4*, 103–109.
(36) Edwards, H. G. M.; Johnson, A. F.; Lawson, E. E. *J. Mol. Struct.* **1995**, *351*, 51–63.
(37) Takumi, N.; Yorinao, I.; Xiao-Song, T. *Biochemistry* **1999**, *38*, 399–403.
(38) Lee, N.-S.; Hsieh, Y.-Z.; Paisely, R. F.; Moris, M. D. *Anal. Chem.* **1988**, *60*, 442–446.
(39) Smithgall, T. E.; Harvey, R. G.; Penning, T. M. *J. Biol. Chem.* **1988**, *263*, 1814–1820.
(40) Rao, T. N.; Yagi, I.; Miwa, T.; Tryk, D. A.; Fujishima, A. *Anal. Chem.* **1999**, *71*, 2506–2511.
(41) Raj, C. R.; Ohsaka, T. *Electrochem. Commun.* **2001**, *3*, 633–638.
(42) Raj, C. R.; Tokuda, K.; Ohsaka, T. *Bioelectrochem.* **2001**, *53*, 183–191.

AM1000213